Dewetting of Ni silicide thin film on Si substrate: In-situ experimental study and phase-field modeling

Jianbao Gao, Annie Malchère, Shenglan Yang, Andrea Campos, Ting Luo, Khalid Quertite, Philippe Steyer, Christophe Girardeaux, Lijun Zhang, Dominique Mangelinck

Dewetting of Ni silicide thin film on Si substrate: In-situ experimental study and phase-field modelling

Jianbao Gao[1,2], Annie Malchère[3], Shenglan Yang[2,4], Andrea Campos[5], Ting Luo[1,6], Khalid Quertite[1], Philippe Steyer[3], Christophe Girardeaux[1], Lijun Zhang[2,*], Dominique Mangelinck[1,**]

[1] Aix Marseille Univ, Université de Toulon, CNRS, IM2NP, Faculté de Saint-Jérôme, 13397 Marseille, France
[2] State Key Laboratory of Powder Metallurgy, Central South University, 410083 Changsha, Hunan, P.R. China
[3] Univ Lyon, INSA Lyon, UCBL, CNRS, MATEIS, UMR5510, 69621 Villeurbanne, France
[4] Department of Energy Conversion and Storage, Technical University of Denmark, 2800 Kgs. Lyngby, Denmark
[5] Aix Marseille Université, CNRS, Centrale Marseille, FSCM (FR1739), CP2M, 13397 Marseille, France
[6] Current address: Max-Planck-Institut für Eisenforschung GmbH, Max-Planck Straße 1, 40237, Düsseldorf, Germany

*Corresponding author: Lijun Zhang, E-mail: lijun.zhang@csu.edu.cn
**Corresponding author: Dominique Mangelinck, E-mail: dominique.mangelinck@im2np.fr

Abstract

In this paper, the *in-situ* Scanning Electron Microscopy (*in-situ* SEM) technique and three-dimensional (3-D) phase-field simulation were combined to perform a comprehensive study on the kinetics and mechanisms of dewetting (or agglomeration) of a 30 nm NiSi films on Si(100) substrate at 600°C. The evolution of texture during agglomeration of the polycrystalline NiSi thin film was also studied by *ex-situ* Electron BackScattered Diffraction (EBSD). The phase-field simulation results showed that abnormal grain growth plays an important role in the dewetting process of polycrystalline films, while the misorientations between NiSi grains and the Si substrate are the main reason for the agglomeration of NiSi polycrystalline thin film on the monocrystal Si substrate. Moreover, 3-D phase-field simulations coupled with experimental information on misorientation distribution and initial grain size were also performed, and the simulated Ni silicide grain morphology is in good agreement with the *in-situ* SEM results during agglomeration. In order to slow down or to suppress the agglomeration, it is highly recommended to either increase the volume fraction of low angle grains, or decrease the misorientation of the NiSi grain/Si substrate or the NiSi grains.

Keywords: NiSi thin film, Dewetting, *in-situ* SEM, Phase-field simulation, Texture, Misorientation

1. Introduction

With the downscaling of microelectronic devices, the Ni monosilicide (NiSi) has been widely used as contacts for the source, drain, and gate in the complementary-metal-oxide-semiconductor (CMOS) transistors. Compared to the former contact materials ($CoSi_2$ and $TiSi_2$), NiSi has attractive advantages, including a lower resistivity, less Si consumption, and Ni diffusion-controlled growth [1]. However, a major disadvantage of the NiSi films is that they are not stable at high temperatures. Indeed NiSi films can quickly degrade during post-formation thermal treatment [2]. Two degradation mechanisms can be distinguished: *i*) in the morphological degradation, the agglomeration (or dewetting) of NiSi occurs upon annealing (when $T \geq 500^{o}C$ depending on the film thickness: the smaller the thickness, the lower the temperature). *ii*) in the phase degradation, NiSi transforms into the high resistivity $NiSi_2$ phase at a higher temperature (around 750~800^{o}C) [3]. For thin NiSi films, such as the ones with a thickness smaller than 30 nm, it has been shown that agglomeration, i.e., that the thin NiSi film breaks up into small islands, occurs at much lower temperatures than the formation of the $NiSi_2$ phase [3]. The agglomerated film then consists of small islands of low resistive NiSi separated by the high-resistive silicon, destroying the low resistance of the contact [4]. In order to avoid this detrimental behavior, there is an urgent need to improve the morphology stability of NiSi films.

Over the last two decades, several experimental studies have been devoted to the factors affecting the agglomeration and phase stability of NiSi films, including heat treatment process [3, 5], thickness of film [3, 6], nature of substrates [3, 7], texture of NiSi grains [3, 4, 8-10], grain growth [11], and alloying elements or impurities [2, 6, 12-15]. Among the factors affecting the agglomeration of the NiSi film, the texture of NiSi grains has been found to play a crucial role in the morphological stability of a thin NiSi film [4].

As the NiSi phase is formed *via* solid-state reaction, the texture inheritance from a precursor phase may benefit the new phase and has been proposed to explain the preferred orientation of NiSi grains [4, 16]. Actually, the NiSi films on monocrystal Si substrates are strongly textured. There are four types of texture components identified in the NiSi film, i.e., *i*) random texture for which no preferential orientation is present in the film; *ii*) epitaxy or in-plane texture for which the orientation between the NiSi grains and the substrate is completely fixed, and there is a two-dimensional match between the film and the substrate at the interface, *iii*) fiber texture, where one of the (hkl) planes is oriented (nearly) parallel to the film/substrate interface, and the NiSi grains are randomly rotated around the axis perpendicular to the interface, i.e., the fiber

axis, that is normal to the surface. *iv*) axiotaxy [17], which can be understood as an off-normal fiber texture (i.e., that the fiber axis is not perpendicular to the interface). The latter texture type, axiotaxy, was revealed on the NiSi films and is due to the match between the spacings (or the projected spacing) of a substrate plane and a film plane [17]. In this case, the interface between the film and the substrate shows a one-dimensional (1-D) periodicity. The axiotaxy texture is common in NiSi films [8-10].

De Schutter *et al*. [4] have reviewed the effect of texture on agglomeration: they emphasized that the minimization of interface energy is the main driving force for agglomeration and examined the contribution of the different textures. Epitaxial grains have an excellent interface match with the substrate, and thus the lowest interfacial energy, unlike those with different textures which have different interfacial energies. Axiotaxial grains still have a decent interface match due to the 1-D periodicity, although slightly worse than epitaxy, and thus medium interfacial energies, while the random grains have the highest interfacial energies. Therefore, there is a driving force for axiotaxial and epitaxial grains to consume neighbor grains with random orientation. However, for epitaxial grains, the interface with the lowest interfacial energy corresponds to a plane-to-plane matching: it is thus difficult to curve the interface since this destroys the matching interface and increases the interface energy. Therefore, the epitaxial grains can only increase their size by lateral growth while keeping the flat interface [4]. For axiotaxial grains, due to the 1-D periodicity interface with the substrate, the curving of the interface does not cost much interface energy, and previous TEM results have shown that the axiotaxial grains indeed have a curved interface in the agglomerated film [17].

For the axiotaxy textured NiSi film on monocrystal Si substrates, there are four common types of NiSi planes parallel to the Si(220) plane: NiSi(211), NiSi(202), NiSi(103), NiSi(112) [17]. De Keyser *et al.* [8] have measured the volume fraction for axiotaxy texture, and they found that the volume fraction of grains for the four axiotaxial texture components is around 40% for two NiSi films with a thickness of 60 nm and 90 nm capped with a 2 nm Si film.

De Keyser *et al.* [9] have also studied the texture evolution during agglomeration by annealing at 550^{o}C for 72 hours of a 60 nm NiSi film obtained by reaction of a Ni film and Si substrate without Si cap: the XRD pole figures show the increase of the axiotaxial and epitaxial components and the decrease of random components after annealing [9]. More precisely, the Electron BackScattered Diffraction (EBSD) results showed that the volume fraction of axiotaxy components increased from 24% to 30% after annealing [9]. It was argued that the axiotaxial grains promote agglomeration. Moreover, Deduytsche *et al.* [14] found that additional alloying elements, such as Ti, W, and Ta, change the texture of thin film by suppressing the axiotaxial

grains and promoting the epitaxial ones. These changes in texture can increase the morphology stability of NiSi film at high temperatures. More recently, Luo *et al.* [18] studied by atom probe tomography the agglomeration of NiSi thin film using Si isotopes enriched multilayers. They found that the diffusion of Si (the slow-diffusing species) along the NiSi/Si interface plays a significant role in the agglomeration of NiSi thin films. Though there is noticeable progress in understanding the agglomeration mechanism of NiSi film and more generally of polycrystalline thin films [3, 4, 8, 9, 18], these mechanisms are still not fully understood. Moreover, the morphological stability and the related effect of texture of NiSi film have been mainly studied by the static experiments (*ex-situ*), such as X-Ray Diffraction (XRD) pole figure, EBSD, Scanning Electron Microscopy (SEM), Transmission Electron Microscope (TEM). A few *in-situ* experiments were performed, such as *in-situ* XRD [3], and *in situ* sheet resistance measurement [19]. However, with these experimental techniques, it is still difficult to study the mechanisms, the complete dynamic evolution, and the kinetics of agglomeration to obtain a good understanding of the agglomeration process. Accordingly, there is an urgent need to develop an appropriate approach to remedy the situation.

Nowadays, the *in situ* experimental observation coupled with the phase-field simulation may serve as an efficient way to bring insights into complex phenomena. I*n situ* observations, such as the ones done in an environmental SEM, can provide direct and reliable data to study the mechanisms and the kinetics of agglomeration. With respect to the phase-field simulation of agglomeration in NiSi films, Bouville *et al*. [20, 21] developed a phase-field method to study grain boundary grooving and agglomeration of a NiSi polycrystalline thin film where each alloy component has a unique diffusivity. They also examined the effect of introducing a slow-diffusing species (Pt) into the film, and the effect of grain shape on the agglomeration of polycrystalline thin films [21]. However, Bouville's work only considers two grains in a 2-D simulation along the longitudinal section, and it cannot completely and quantitatively describe the evolution of agglomeration. Moreover, such a simple model does not consider the effect of texture. In order to perform a quantitative simulation of the agglomeration (or dewetting) phenomenon and to study the effect of texture on NiSi thin films, the 3-D multi-phase-field (MPF) model is required. This type of simulation has emerged as a powerful tool to simulate the microstructural evolution in various materials processes during their lifetime [22-27]. It can be utilized by coupling with reliable CALPHAD (calculation of phase diagram) thermodynamic and atomic mobility databases [24].

Consequently, in this work, *in-situ* SEM observations and MPF simulations are combined to investigate the mechanism of agglomeration in the polycrystalline NiSi thin film. The

agglomeration kinetics and the morphological evolution of the NiSi thin film are determined by *in-situ* high-temperature SEM observations, while the evolution of texture for the polycrystalline NiSi thin film during agglomeration is studied by *ex-situ* EBSD. The 3-D phase-field simulation is performed by considering the orientation of both NiSi grains and Si substrate. The effect of misorientation on the agglomeration is quantitatively investigated, to reproduce the results of *in-situ* SEM. The role of the NiSi grain orientation is highlighted.

2. Experimental procedure

A 15 nm thick Ni film was deposited at room temperature by magnetron sputtering onto (100) Si substrates. The Si(100) substrates were immersed into a 5% HF solution for 1 min to remove the native oxide prior to the deposition. The deposition was performed in a sputtering deposition system with a base pressure of 10^{-8} Torr using 99.99% pure Ar gas flow. The wafer was mounted on a rotating sample holder to obtain a homogeneous deposit. The deposition rate as a function of power was calibrated for the Ni target. The applied power on the Ni target is 50W and the corresponding deposition rate is 0.136 nm/s. According to the conservation of the mass of Ni atoms, the full consumption of the 15nm Ni film by solid state reaction with the silicon substrate will result in a NiSi film of about 30 nm.

In situ hot stage scanning electron microscopy has been done using an environmental SEM FEG QUATTRO (Thermo Scientific). A 3mm×3mm sample consisting of a 15nm Ni film deposited on Si substrate, was introduced into a MgO crucible mounted, in the SEM, on a furnace capable of reaching 1000°C. Heating was done in vacuum mode, in order to avoid oxidation of the Ni film. The sample was heated with the following ramp: 30 K.min^{-1} up to 450°C, 10 K·min^{-1} up to 550°C, and finally slowly (5 K·min^{-1}) till 600°C. Then the sample was held at 600°C for almost 4 hours (238 min). Observations were done at 10 kV, in order to finely see grains in the Ni layer with an Everhart-Thornley Detector. Pictures were taken every 1 or 2 minutes in order to build the detailed kinetic curves afterward. The evolution of phase area fraction was deduced after treatment of image stack in ImageJ software.

Rapid thermal processing (RTP) was used for annealing sample at 600^{o}C for 60 s under vacuum (~10^{-6} mbar) with the ramp rate as nearly 50^{o}C/s. A long-time annealing sample was prepared by vacuum annealing furnace (the ramp rate is nearly 0.57^{o}C/s) under vacuum (10^{-7} mbar) at 600^{o}C for 24 hours. The structure of the films was investigated using X-ray diffraction (XRD) in the θ-θ geometry using a Cu Kα source ($\lambda_{K\alpha}$ = 0.154 nm). The NiSi grain orientation maps were collected using the EBSD technique in a Zeiss Gemini 500 field-emission gun scanning electron microscope (FEG-SEM) equipped with an EDAX Hikari Super acquisition

system. EBSD scans were performed at 12 kV accelerating voltage, using step sizes between 20 and 50 nm. Post-processing analysis of the EBSD data was performed using the OIM Analysis™ software [28], combined with the MTEX Toolbox [29] for texture analysis and visualization. Low kV images were taken with this Zeiss FEG-SEM, using two secondary electrons (SE) detectors: an InLens SE detector (located inside the electron column) that provides high-resolution surface structure and an Everhart-Thornley SE detector, used for topography observation.

3. Multi-phase-field (MPF) modeling

3.1 MPF models

In this work, the contribution of the elastic field was not taken into account. Under this assumption, the total energy functional can be generally divided into the interfacial part f^{intf} and chemical part f^{chem} [30, 31]:

$$\mathrm{F} = \int_{\Omega} f^{\text{intf}} + f^{\text{chem}} \tag{1}$$

$$f^{\text{intf}} = \sum_{\alpha,\beta=1,\ldots,N} \frac{4\sigma_{\alpha\beta}}{\eta}\left\{-\frac{\eta^2}{\pi^2}\nabla\phi_\alpha\cdot\nabla\phi_\beta + \phi_\alpha\cdot\phi_\beta\right\} \tag{2}$$

$$f^{\text{chem}} = \sum_{\alpha=1,\ldots,N} h(\phi_\alpha) f_\alpha(c_\alpha^i) + \tilde{\mu}^i\left(c^i - \sum_{\alpha=1,\ldots,N}\phi_\alpha c_\alpha^i\right) \tag{3}$$

where N = N(x) is the local number of phases, ϕ_i is the phase-field value of α phase/grain, the condition $0 \le \phi_i \le 1$ and the sum constraint $\sum_{\alpha=1,\ldots,N}\phi_i = 1$ are always fulfilled, and $\sigma_{\alpha\beta}$ is the interface energy between phases/grains α and β. It can be anisotropic with respect to the relative orientation between the phases/grains. $\eta_{\alpha\beta}$ is the interface width and is treated to be equal for all interfaces. There are two terms in the brace of Eq.(2), i.e., $-\frac{\eta^2}{\pi^2}\nabla\phi_\alpha\cdot\nabla\phi_\beta$ corresponding to the gradient term between two phases/grains α and β, while $\phi_\alpha\cdot\phi_\beta$ the double obstacle potential. In Eq.(3), $f_\alpha(c_\alpha^i)$ is the bulk free energy density of the individual phase, which depends on the phase concentrations c_α^i, and can be obtained from the reliable thermodynamic database. The interpolating function $h(\phi_\alpha)$ is an arbitrary function which is defined changing monotonously from $h(0) = 0$ to $h(1) = 1$. Such a function is introduced to avoid the driving forces in the bulk region, but also to enhance numerical stability in applied computations. In most cases, the function is taken as: $h(\phi) = \phi$. $\tilde{\mu}^i$ is the diffusion potential of the component i introduced as a Lagrange multiplier to conserve the mass balance between the phases

$c^i = \sum_{\alpha=1,\ldots,N} \phi_i c_\alpha^i$. The chemical part f^{chem} depends on the sum of the bulk free energy density $f_\alpha(c_\alpha^i)$ of all phases and the contribution of diffusion potential $\tilde{\mu}^i$.

Based on the free energy functional shown in Eqs.(1) ~ (3), the MPF evolution equations can be then derived based on the above free energy functional [30-32]:

$$\dot{\phi}_i = \sum_{\beta=1,\ldots,N} \mu_{\alpha\beta} \left\{ \sigma_{\alpha\beta} \left[\phi_\beta \nabla^2 \phi_\alpha - \phi_\alpha \nabla^2 \phi_\beta + \frac{\pi^2}{2\eta_{\alpha\beta}^2} (\phi_\alpha - \phi_\beta) \right] + \frac{\pi}{\eta_{\alpha\beta}} \sqrt{\phi_\alpha \phi_\beta} \Delta g_{\alpha\beta} \right\} \quad (4)$$

$$\dot{c}^i = \nabla \sum_{\alpha=1,\ldots,N} \sum_{j=1,\ldots k} \phi_\alpha D_\alpha^{ij} \nabla c_\alpha^j \quad (5)$$

$\mu_{\alpha\beta}$ is interfacial mobility between the α and β phases. In Eq.(4), the evolution of the phase field ϕ depends on two terms, i.e., the first curvature term $\left(\phi_\beta \nabla^2 \phi_\alpha - \phi_\alpha \nabla^2 \phi_\beta + \frac{\pi^2}{2\eta_{\alpha\beta}^2} (\phi_\alpha - \phi_\beta) \right)$, and the second driving force term $\Delta g_{\alpha\beta}$. $\Delta g_{\alpha\beta}$ is the local deviation from thermodynamic equilibrium given as

$$\Delta g_{\alpha\beta} = -f_\alpha(c_\alpha^i) + f_\beta(c_\beta^i) + \tilde{\mu}^i (c_\alpha^i - c_\beta^i) \quad (6)$$

It should be noted that the chemical driving force $\Delta g_{\alpha\beta}$ can be obtained by linking to the real CALPHAD thermodynamic databases through the TQ-interface of Themo-Calc software [33]. D_α^{ij} represents the multi-component diffusion matrix for all phase α and all solute interaction ij. Actually, Eq.(4) cannot be directly derived from the free energy functional, but is a so-called antisymmetric approximation, which resigns from thermodynamic consistency at the multiple junctions [31, 32]. This is commonly done in most simulations using the MPF model [32], and has been incorporated in the MICRESS (MICRostructure Evolution Simulation Software) code [34], which will be utilized for the present phase-field simulation.

3.2 Materials parameters

The prerequisite for a quantitative phase-field simulation is to link the phase-field code to the CALPHAD thermodynamic and atomic mobility databases, in order to provide realistic chemical driving force, diffusion potentials, and chemical mobility/diffusivity at any composition and temperature. It should be noted that the chemical driving force $\Delta g_{\alpha\beta}$ can be obtained by linking to the real CALPHAD thermodynamic descriptions, while M_α is the chemical mobility in the α phase and can also be directly obtained from the CALPHAD atomic mobility descriptions.

For the Ni-Si system, the thermodynamic descriptions from *Du* and *Schuster* [35, 36] were employed to provide the chemical driving force and diffusion potentials during the present phase-field simulation. As we only study the agglomeration at low temperatures, there is no phase transition from the NiSi phase to the $NiSi_2$ phase since the nucleation of $NiSi_2$ usually occurs above 750°C [37]. Thus, only the NiSi and (Si) phases were considered in the simulation. Each phase should obey the conservation of volume or mass during the agglomeration. In order to respect the conservation of volume or mass for the NiSi and (Si) phases in the simulation, an extremely tiny solid solubility of the (Si) phase was set manually in the thermodynamic descriptions (see in Table S1), and then the initial composition of the (Si) phase was set as the solid solubility limit at the corresponding temperature (see in Figures S1 and S2).

Concerning the atomic mobility, Luo *et al.* have shown that the diffusion along with the interface of the slow diffusion Si species is crucial for the agglomeration process, and the diffusion of Si at the NiSi/Si interface $D^{Si}_{NiSi/Si}$ was roughly estimated as 1×10^{-11} cm^2/s at 600°C [18]. This value is about 4 orders of magnitude larger than the self-diffusion of Si in NiSi [18, 38], and 14 orders of magnitude larger than the self-diffusion of Si in Si (i.e., 2×10^{-25} cm^2/s) [39]. Thus, only the value of Si diffusion along the NiSi/Si interface is considered in the simulation.

Moreover, reliable thermophysical parameters are also critical for performing the quantitative phase-field simulation. Two important interfacial energies are the NiSi/Si interfacial energy ($\sigma_{NiSi/Si}$) and the NiSi grain boundary energy ($\sigma_{NiSi/NiSi}$). However, no reported data are available for the two interfacial energies. Since the high-angle grain boundary energies of metals are often found to be roughly 1/3 of their surface energies [40], the NiSi grain boundary energy can be roughly estimated to 1/3 of its surface energy. Recently, Luo *et al.* have observed the triple junction with NiSi-Si-vacuum by the APT (Atom Probe Tomography) under the equilibrium state [18]. From this observation and the known Si surface energy, the NiSi surface energy and the NiSi/Si interface energy can be thus calculated. As the Si surface energy ranges from 0.84×10^{-4} J/cm^2 to 1.90×10^{-4} J/cm^2 for different cleavage-surfaces [41], the value of 1.90×10^{-4} J/cm^2 for the Si surface energy corresponding to the (110) plane, has been used in this work since it corresponds to the (110) plane, which is often observed in the axiotaxial texture. Therefore, the NiSi surface energy and the NiSi/Si interface energy were evaluated to be 1.8×10^{-4} J/cm^2 and 4.94×10^{-5} J/cm^2, respectively. Furthermore, the NiSi grain boundary energy was taken as 6.0×10^{-5} J/cm^2 (i.e., 1/3 of the NiSi surface energy). The interfacial mobility between different interaction pairs was evaluated according to Eq.(35) in Ref. 33 to achieve a

diffusion-control process. All the simulation parameters used in this work are listed in Table S2.

In order to study the effect of texture on the agglomeration (or dewetting), the interfacial energy and interfacial mobility for cubic phase Si and the orthorhombic NiSi phase were considered to be dependent on the interface misorientation. The reduction of interfacial energy as a function of misorientation angle θ was taken to be governed by the Read-Shockley law [42] implemented in MICRESS:

$$\sigma(\theta)=\sigma_{HAB}\frac{\theta}{\theta_{HAB}}\left[1-\ln\left(\frac{\theta}{\theta_{HAB}}\right)\right] \quad (7)$$

where σ_{HAB} and θ_{HAB} are the interfacial energy of a high angle grain boundary and the misorientation corresponding to the transition angle between low and high angle grain boundaries. The reduction of interfacial mobility as a function of the misorientation was taken to be described by the sigmoidal law suggested by Humphreys [43]:

$$\mu(\theta)=\mu_{HAB}\left(1-\exp\left[-B\left(\frac{\theta}{\theta_{HAB}}\right)^{n}\right]\right) \quad (8)$$

where μ_{HAB} is the interfacial mobility of a high angle grain boundary, B and n are two model parameters usually set to B=5 and n=4. Figure S3 shows the curve form of Eq.(7) and Eq.(8) with θ_{HAB}=15°. In the present phase field simulations, the orientation of each grain was defined by Euler angle, and the misorientation θ between NiSi grains and Si substrate, as well as that between neighbor NiSi grains, was calculated. Then, $\sigma(\theta)$ and $\mu(\theta)$ for each interface were calculated based on the Eq.(7) and Eq.(8) with the transition angle θ_{HAB} =15°, and used in the phase-field evolution equation (i.e., Eq.4) for describing the evolution of phase field. For the NiSi grain, different interfaces have different interfacial energies and mobilities, which depend on the misorientation between two grains or phases on both sides of the interface.

4. Experimental results

4.1 Microstructure evolution observed by the in-situ SEM

Figure 1 shows low magnification SEM images of a 30 nm NiSi film on Si(100) substrate *in-situ* heating at 600°C. Different phases could be distinguished from the contrast in the SEM images. The white and gray regions respectively correspond to the big NiSi grains and the smaller ones, while the black region is the exposed Si surface (the green region indicates dust on the sample surface). **Fig. 1a** shows the NiSi thin film morphology after 23 min annealing at

600°C. The agglomeration of NiSi thin film is at the beginning stages, as indicated by small black regions of Si. The initial NiSi grains are small and close to each other. With increasing the annealing time from 23 min to 32 min, most NiSi grains gradually shrink (small grains in grey), while some specific NiSi grains grow rapidly, appearing as large grains in white (**Fig. 1b**). Meanwhile, the fraction of exposed Si increases. With the agglomeration process, the expansion direction of the exposed Si depends on the consumption of the small NiSi grains, as the large NiSi grains achieve a slow-growing stage and stop the expansion of the exposed Si (**Fig. 1(c-d)**). This shows that the agglomeration of the NiSi grains causes an increase in the exposed Si. Due to the large contrast between NiSi and Si (grey/white *vs.* black) and because of the difficulty to separate the grey level associated with the NiSi grains, the kinetic of the exposed Si would be used to study the agglomeration kinetics of the NiSi thin film on the Si(100) substrate.

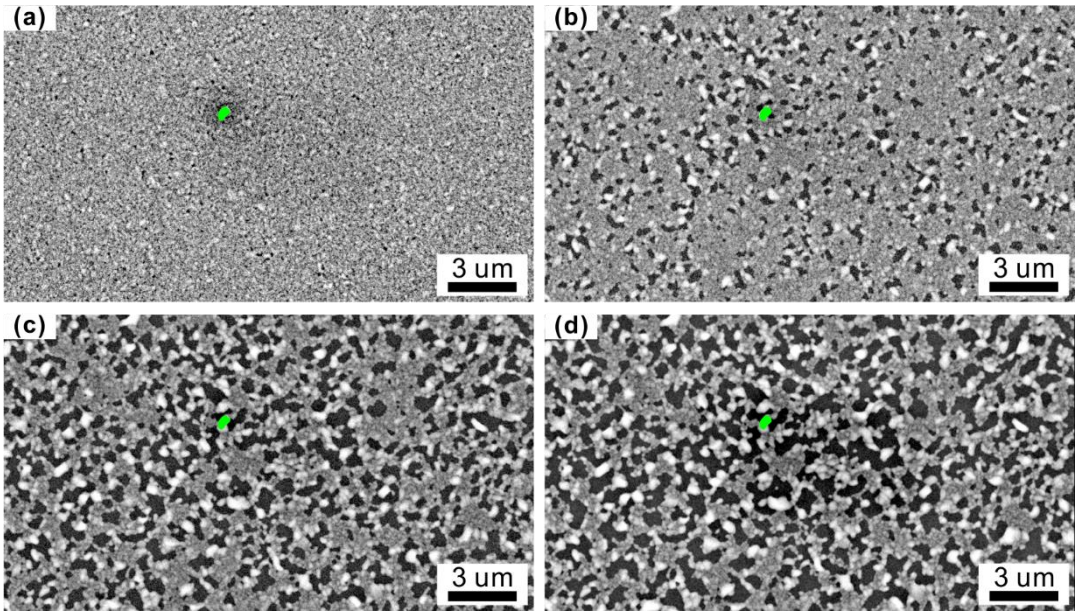

Fig. 1. SEM images showing microstructure evolution with time of the same area, during *in-situ* heating at 600°C, of a 15nm Ni thin film on Si(100) substrate: (a) 23 min (b) 32 min (c) 194 min (d) 287 min. The white and gray regions are the NiSi phase, the black phase is the exposed Si surface. (the green region reveals dust on the surface's sample).

4.2 Agglomeration kinetics

Figure 2 shows the kinetic of the exposed Si relative to a 15 nm Ni film deposited on Si(100) substrate annealing at 600°C determined from *in-situ* SEM results. As shown in **Fig. 2a**, the fraction of the exposed Si increases very slowly before 23 min, but then increases quickly following a power function (the details will be introduced later). **Fig. 2a** also shows that the number of exposed Si regions (blue curve, right axis) first increases fast to reach a maximum,

then decreases slowly and tends to a stable value. During the heating stage, it takes 40 min to reach 600°C, as shown in Figure S4. However, the agglomeration of NiSi grains happens already before the temperature reaches 600°C, i.e., before 40 min. Prior to the agglomeration of NiSi, solid state reaction between Ni thin film and Si substrate to form NiSi as well as the grooving at the grain boundaries of NiSi have also happened during the heating process. Thus, it is difficult to know the accurate starting time of agglomeration and to compare agglomeration kinetics with other experimental results from different holding temperatures or samples. In addition, the exposed Si fraction is too small to be accurately determined at these initial stages. Therefore, we prefer not to take into account the early stage and to start at a time corresponding to a given f_0(e-Si) value, representing the initial fraction of the exposed Si that can be easily measured. The value of f_0(e-Si) of 3 % was selected in our work and the time-shifted kinetics (corresponding to a time shift of about 26 min) of the exposed Si are shown in **Fig. 2b**. When the area fraction of exposed Si reaches 3 %, the temperature is around 550°C (26 min), which is not so far from 600°C, the detail is shown in Figure S4.

The shifted kinetics of exposed Si for a 15 nm Ni thin film on Si(100) substrate for two experiments with different magnifications (Exp-1: low-magnification with area=303 μm^2 and Exp-2: high-magnification with area=20.3 μm^2 - see in Figure S5) are shown in **Fig. 2b**. In order to assess the error of the area fraction of exposed Si, each image from the low-magnification *in-situ* SEM experiment (Exp-1 with a total area of 303 μm^2: 23 μm×13 μm) was randomly divided into 120 regions, which size is the same as the high-magnification *in-situ* SEM experiment (Exp-2 with a total area of 20.3 μm^2: 5.4 μm×3.8 μm). The exposed Si area fraction was determined for each of these regions to obtain the average, minimum, and maximum of this value. In **Fig. 2b**, the orange line represents the average area fraction and the orange region represents the measurement error from maximum and minimum. **Fig. 2b** shows that the kinetics from the high-magnification *in-situ* experiment is within the error range of the low-magnification *in-situ* experiment. Moreover, the average area fraction of exposed Si can be well fitted by a power function ($y=a\cdot x^b$, where a is 7.7 and b is 0.28, and the fitting goodness, R^2, is 0.972). Therefore, the area fraction of exposed Si for larger f_0(e-Si) than 3 %, increases in a power function.

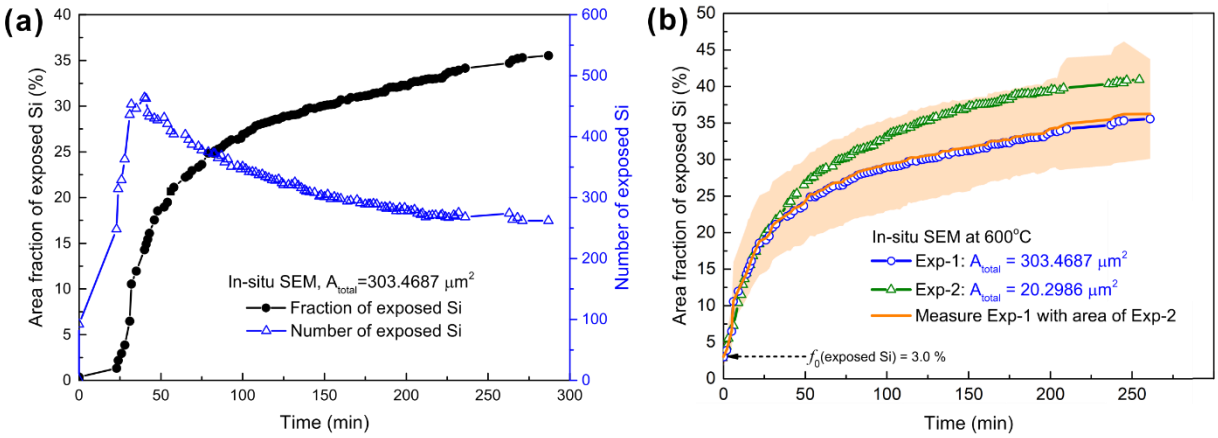

Fig. 2. Kinetic of exposed Si during *in-situ* SEM at 600°C of a 15 nm Ni film on Si(100) substrate: (a) Area fraction and the number of the regions for the surface-exposed Si with time, (b) Shifted kinetics of exposed Si from *in-situ* SEM results with different magnifications (Area=303 μm^2 and Area=20.3 μm^2): the orange region represents the measurement error of the low-magnification experiment (Exp-1 with a total area of 303.47 μm^2) using the same measured size with the high-magnification experiment (Exp-2 with the total area of 20.30 μm^2). This error range is from the maximum and the minimum.

4.3 Long-time annealing

In order to study the different states of NiSi agglomeration, long-time annealing of the 15 nm Ni film on Si(100) substrate was performed at 600°C for 24 hours, and a sample was also annealed at 600°C for 60 s by RTP for comparison.

XRD and low kV SEM images (**Fig. 3**) indicate that there is only the NiSi phase after long-time annealing at 600°C for 24 hours. Furthermore, XRD analysis (not shown) of a sample with vacuum annealing at 400°C for 1 hour was used to ensure that the Ni film is fully transformed to the NiSi well below 600°C. **Fig. 3a** shows the relative intensity of the XRD peak change with annealing time. In particular, there is an increase in the (013) peak intensity that indicates a change in texture. **Fig. 3b** shows the morphology of NiSi that is characteristic of a severe agglomeration with the formation of NiSi islands. The surface morphology and grain boundary of NiSi grains can be clearly observed in **Fig. 3b** zoom image.

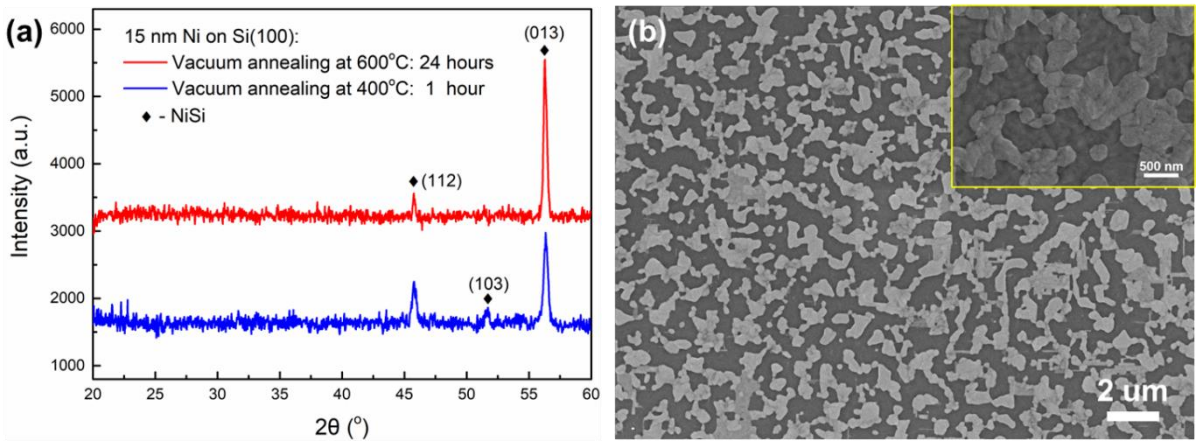

Fig. 3. (a) XRD scan at room temperature and (b) Low kV SEM images for a 15nm Ni film on Si(100) substrate with annealing 24 h at 600°C. The illustration in (b) shows the surface morphology of NiSi.

Figure 4 displays the EBSD orientation maps and pole figures for a 15nm Ni film on Si(100) substrate for 60 s and 24 hours at 600°C. In **Fig. 4a** and **Fig. 4b**, the black region is the Si substrate, and each color represents an orientation of the NiSi grains. After annealing at 600°C for 24 hours, some phenomena can be clearly observed: *i*) a number of small grains have disappeared, and there is a general grain growth with the average grain radius increasing from 137 nm to 193 nm, as shown in **Fig. 4c**, and *ii*) some grains with a particular orientation grow abnormally. Pole figures show that these special grains with particular orientations have similar fiber texture while grains with random orientation disappear, as shown in **Fig. 4d** and **Fig. 4e**. These results are in good agreement with De Keyser's work on 60 nm NiSi films with a dwell time of 72 h at 550°C [9]. These special grains (such as axiotaxy and epitaxy) have smaller interface energy than the random orientation grains due to matching with the Si substrate in one (axiotaxy) or two dimensions (epitaxy): this causes abnormal grain growth during the agglomeration of NiSi grains [4].

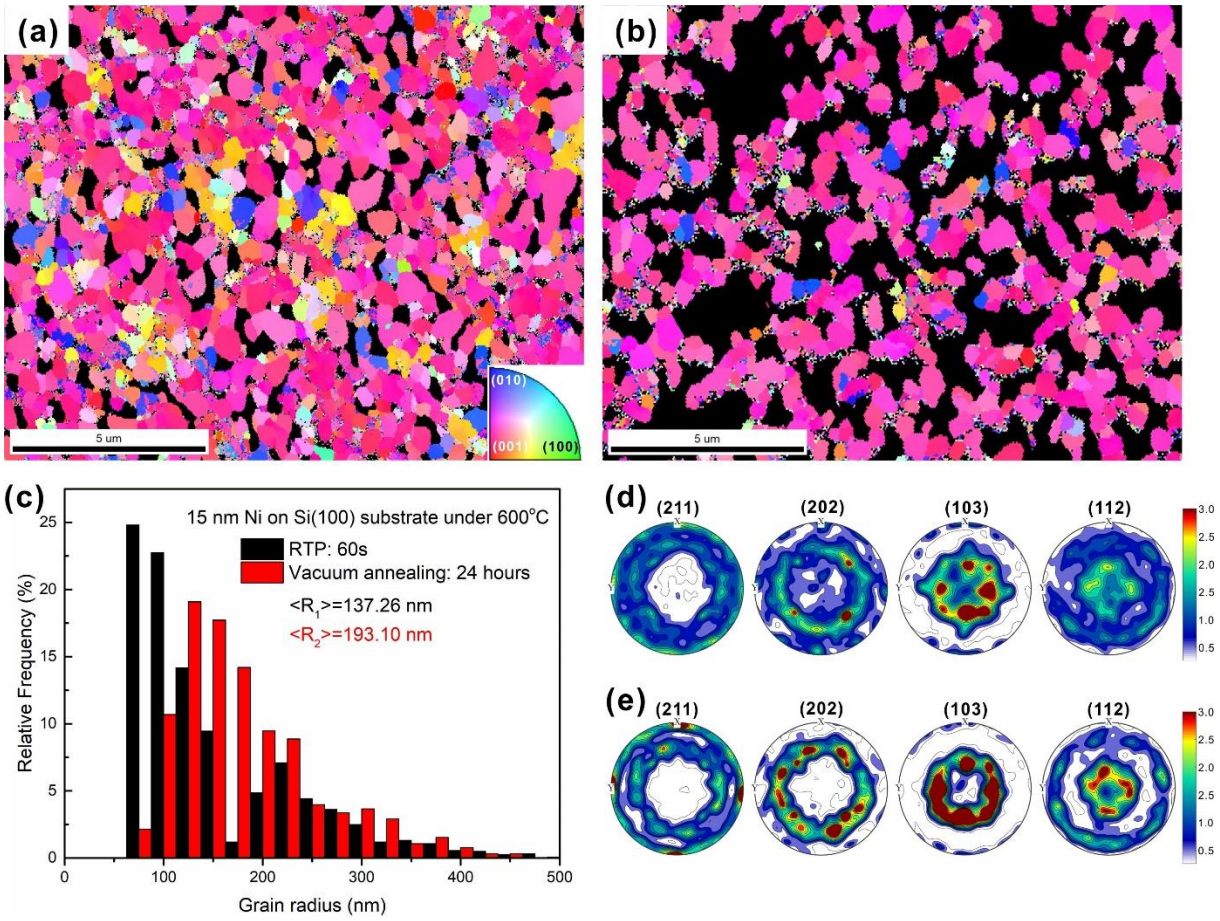

Fig. 4. EBSD orientation maps and pole figures for 15nm Ni film on Si(100) substrate after: (a) RTP at 600ºC for 60 s and (b) vacuum annealing 24 hours at 600ºC. (c) is the grain size distribution. Pole figures for 15nm Ni film on Si(100) substrate are shown in: (d) for RTP at 600ºC for 60 s, and (e) for vacuum annealing 24 hours at 600ºC.

5. MPF simulation results

In order to reveal the mechanism of NiSi agglomeration, the effect of NiSi grains orientation on the agglomeration has been studied by 3D phase-field simulations, focusing on different volume fractions and misorientation distributions of the NiSi grains.

5.1 Effect of NiSi orientation

The driving force for agglomeration is mainly the reduction of interfacial energy (including grain boundary energy) in the system. Misorientation affects the interfacial energy/grain boundary energy and the interfacial mobility between the NiSi grains and the Si substrate. The reduction factors are calculated by Eq.(7) and Eq.(8). **Table 1** lists the NiSi grains orientation types (1 to 4) used in the simulations (A to F groups). Orientation is not considered in type 1 NiSi grains. For the other types, the orientations are defined by the Euler angles. For type 2 NiSi grains, the Euler angles, φ=270º, θ=20º, ψ=90º, noted NiSi(φ=270º, θ=20º, ψ=90º), are

representative of the Euler angles for the NiSi(103) axiotaxy. In order to conveniently study the effect of misorientation on agglomeration, the orientation of type 3 NiSi(φ=270°, θ=35°, ψ=90°) and 4 NiSi(φ=270°, θ=30°, ψ=90°) grains is set as high-angle misorientation grains (HAMG) compared to the type 2 NiSi(φ=270°, θ=20°, ψ=90°) grains. The orientation of Si substrate is also set relative to the type 2 NiSi grains, as Si(φ=270°, θ=25°, ψ=90°). It was chosen to always keep some misorientation between NiSi grains and Si substrate to allow the evolution of the system. Since only θ is changed for all the orientations, we will now use the following simplified notation: type 2 NiSi(θ=20°), type 3 NiSi(θ=35°), type 4 NiSi(θ=30°), and Si(θ=25°). The misorientation limit for high angle boundaries is set to 15° for NiSi/Si and NiSi/NiSi in the simulation. For simulations A to F, the simulated domain is 100×100×40 grids, grid size Δx is 5 nm, and the interface thickness is $4\Delta x$. The thickness of the NiSi film is set to 30 nm, and the initial average grain radius is 85 nm, closing to the *in-situ* SEM experiments at 600°C. Periodic boundary conditions are used along with the four horizontal directions (west, east, south, north), and isolation conditions are used for the top and bottom boundaries in all simulations. Only one set of thermophysical parameters was used in all simulations, which were obtained through reasonable evaluation, as described in *Section* 3.2. The volume fraction of the NiSi phase and the Si substrate are conserved in all simulations. The parameters (interfacial energy and interfacial mobility) used in the simulations A to F are listed in Table S3.

Table 1 Volume fractions of different orientations in NiSi film in the simulations A to F.

Type of NiSi grains	Orientation [Euler angle, (φ,θ,ψ)]	Volume fraction					
		A	B	C	D	E	F
1	--	100	--	--	--	--	--
2*	270°,20°,90°	--	22.65	43.21	69.23	77.25	--
3	270°,35°,90°	--	77.25	56.69	30.67	22.65	69.23
4	270°,30°,90°	--	--	--	--	--	30.67

* NiSi(270°,20°,90°) is one of Euler angle of the axiotaxy NiSi(103).

Figure 5a illustrates the effect of the misorientation on the agglomeration of NiSi film from the present phase-field simulations. Firstly, in simulation A, all NiSi grains are isotropic without orientation. The evolution of NiSi grains is then controlled by grain growth and interface diffusion, as shown in **Fig. 5a**. Indeed, **Fig. 5a** shows that grooving and agglomeration happen and lead to the isolated NiSi islands. Then some islands grow at the expense of the other and

finally form a big isolated island. The kinetic of the exposed Si fraction for simulation A is shown in **Fig. 6a**.

In order to check the effect of misorientation and texture on agglomeration, special orientations between the NiSi grain and Si substrate were introduced in other simulations. In simulation B, 77.25% of the NiSi grains are the type 3 with a 10^o misorientation compared to Si substrate (relatively high-angle misorientation-HAM that can be representative of the random orientation grains), and 22.75% are type 2 grains with a 5^o misorientation (low-angle misorientation, LAM, representative of epitaxy or axiotaxy grains). It means that 77.25% of NiSi grains (HAMG) have higher interfacial energy and mobility than the other grains (low-angle misorientation grains-LAMG). Note that the interfacial energy and mobility between the same type NiSi grains are close to 0 due to the 0^o misorientation. **Figure 5b** shows the evolution of the microstructure for simulation B (the HAMG are in red and the LAM ones in orange): the abnormal grain growth of the LAM NiSi grains is clearly observed, and the evolution of HAMG is faster than the LAMG. This phenomenon is very similar to the *in-situ* SEM results. Moreover, the kinetics of the exposed Si fraction of simulation B with orientated grains is close to the *in-situ* results, as shown in **Fig. 6a**. It is slower than simulation A with isotropic grains. By comparing the results of simulations A and B, it is clearly found that the misorientation between the NiSi grains and the Si substrate and the one between the NiSi grains strongly affect the agglomeration of the NiSi film by affecting the interfacial energies and mobilities. Furthermore, as the effect of misorientation on the agglomeration of NiSi is dependent on the volume fraction and misorientation distribution, more phase-field simulations will now be presented to study these factors.

5.2 Effect of the different volume fractions of different orientations

In order to study the effect of different volume fractions of NiSi orientations on agglomeration, simulations (B to E) with different volume fractions of NiSi orientations but with the same NiSi grain structure were performed (**Fig. 5b-e**). Two types of NiSi grains (misorientations are 5^o and 10^o with Si substrate) with different fractions are set in the simulations B to E, and the volume fraction of the HAM NiSi grains in the NiSi film varies from 77.25% to 22.65%. These simulation results show that the lower fraction of the HAMG, the lower fraction of exposure of Si substrate. **Figure 6a** shows the kinetics of the exposed Si from the *in-situ* SEM and the simulation A to E with shifted time using f_0(e-Si) = 3.0% as the initial time. The kinetics of simulations B to E confirms that a smaller fraction of HAMG slow

down the exposure rate of the Si substrate. It means that the LAMG are efficient in reducing agglomeration. Moreover, the simulations show that when the fraction of HAMG lies between 30.67%~56.70%, the kinetics of the surface-exposed Si are in good agreement with the *in-situ* SEM results. In other words, when the fraction of LAMG is 43.30%~69.33%, the kinetic of the exposed Si obtained by the phase-field simulations reproduce the *in-situ* SEM results.

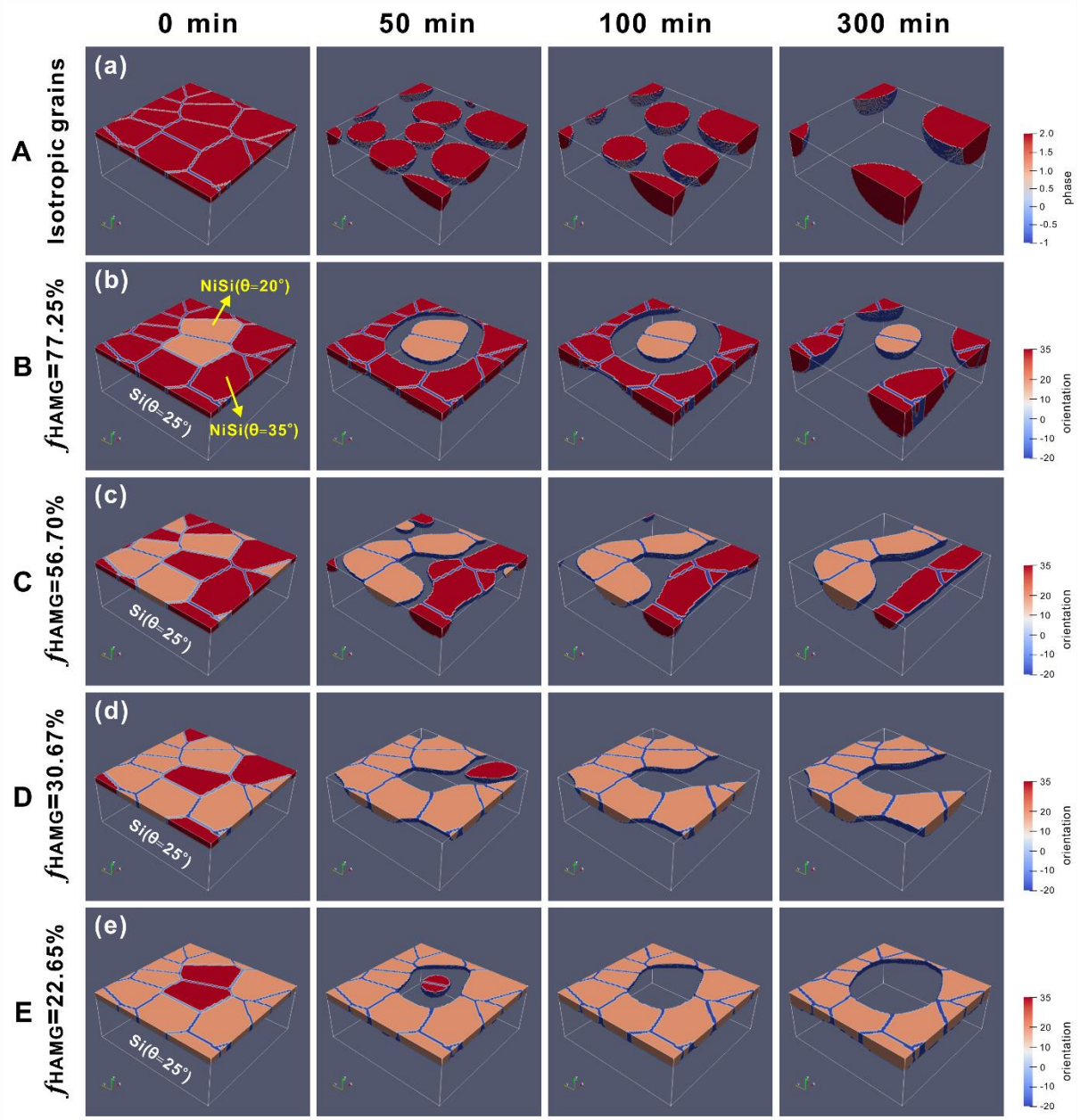

Fig. 5. Simulated microstructure evolution for different high-angle misorientation grains (HAMG) fraction of the agglomeration for a 30 nm NiSi film on Si substrate at 600ºC: (a) isotropic grains, (b) f_{HAMG}=77.25%, (c) f_{HAMG}=56.70%, (d) f_{HAMG}=30.67%, and (e) f_{HAMG}=77.25%. Different colors represent the different NiSi orientations, while the Si substrate is transparent.

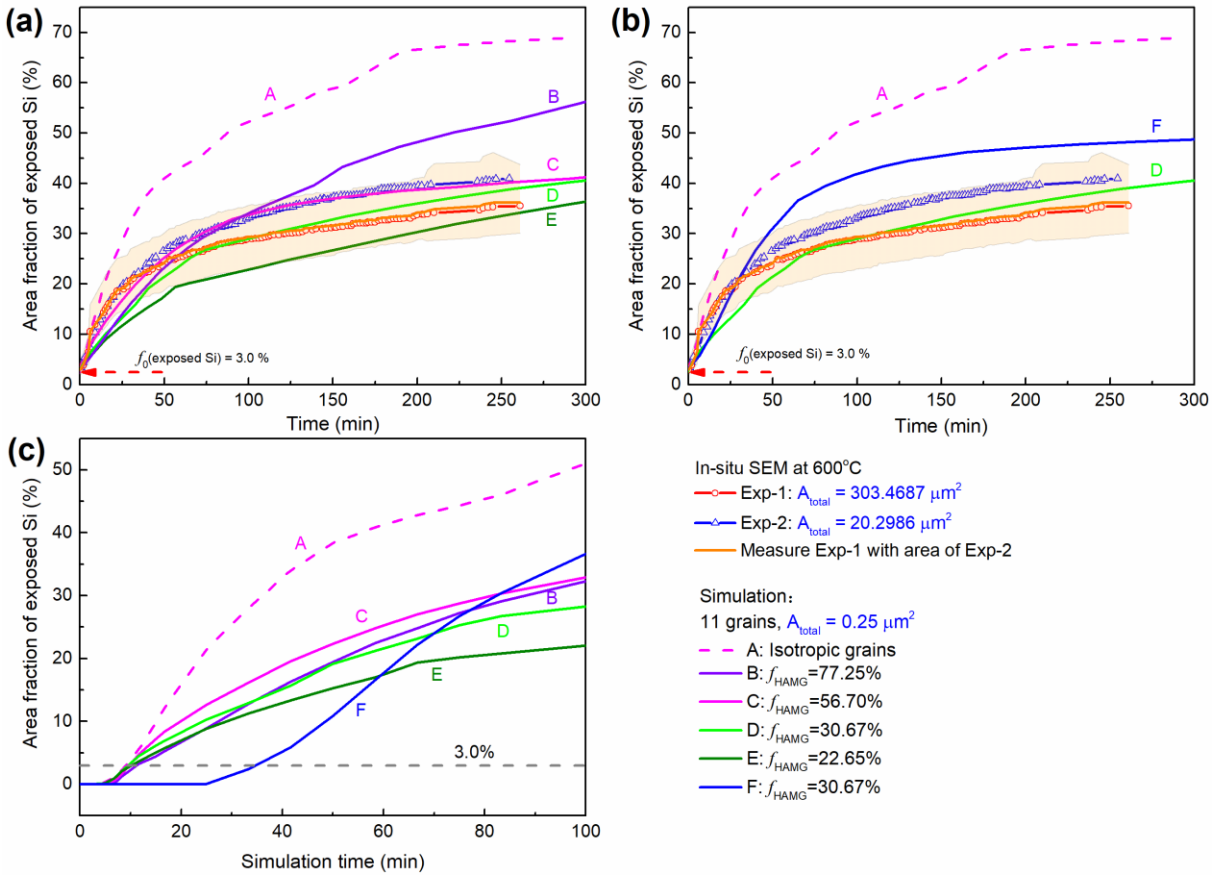

Fig. 6. Kinetics of the exposed Si area fraction with shifted time of *in-situ* SEM and simulated results for a 30 nm NiSi film on a monocrystal Si substrate at 600°C. The area fraction of exposed Si taken as initial time is equal to 3.0% in (a) and (b): (a) simulation A to E groups, (b) simulation A, D, and F groups, (c) simulation A to F during the early stage with a none shifted time.

5.3 Effect of different misorientation distributions

The simulations D and F were performed to study the effect of different misorientation distribution with the same volume fraction on the agglomeration of NiSi grains. In the two simulations, the volume fractions of HAM type 3 NiSi(θ=35°) grains are equal to 30.67%. Type 2 NiSi(θ=20°) grains are LAMG in simulation D with Si(θ=25°) substrate, and type 4 NiSi(θ=30°) are LAMG in simulation F with Si(θ=20°) substrate, the misorientation between NiSi and Si substrate changes from 5° and 10° in simulation D to 10° and 15° in simulation F. Since the Si orientation is different for the two simulations (**Fig. 7**), the misorientation between the NiSi grains also changes from 10 ° to 5° from the simulations D to F. On the one hand, as the total interfacial energy of the NiSi/Si interface increases in simulation F compared to simulation D, the evolution of NiSi grains with the Si substrate should be enhanced. **Figure 6b** compares the kinetics of the exposed Si obtained by *in-situ* SEM with the results of time-shifted simulations A, D, and F: the kinetics of the exposed Si substrate is found to be faster for

simulation F than that for simulation D, as expected. On the other hand, the total energy of NiSi/NiSi grain boundary decreases in simulation F compared to simulation D, and the evolution between NiSi grains with different orientations should be weakened. **Fig. 7a** and **Fig. 7b** for a time of 50 min show that the evolution between NiSi grains with different orientations is indeed weakened in simulation F and slower than in simulation D.

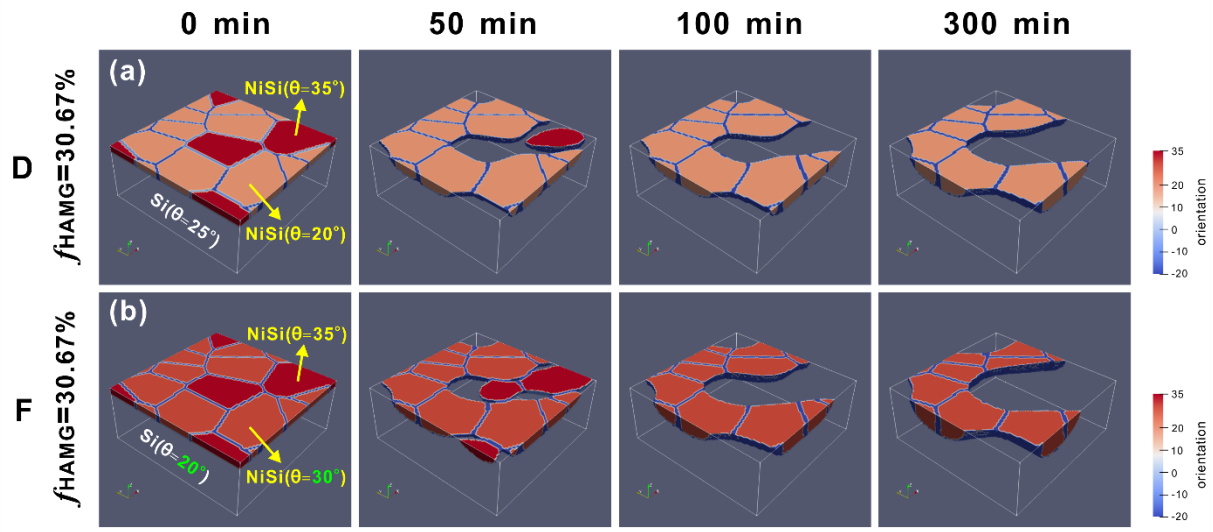

Fig. 7. Simulated microstructure evolution for different misorientation distributions with the same volume fraction on the agglomeration for a 30 nm NiSi film on Si substrate at 600°C: (a) f_{HAMG}=30.67%, with $\theta_{NiSi^2/Si}$ is 5°, $\theta_{NiSi^3/Si}$ = 10°, $\theta_{NiSi^2/NiSi^3}$ = 15°, (b) f_{HAMG} = 30.67%, with $\theta_{NiSi^3/Si}$ = 15°, $\theta_{NiSi^4/Si}$ = 10°, $\theta_{NiSi^3/NiSi^4}$ = 5°. The different colors represent the different NiSi orientations, while the Si substrate is transparent.

5.4 Grooving

Figure 8 shows the evolution of the longitudinal cross-section of the phase-field simulated microstructure with different misorientation distributions but the same volume fraction (simulation D and simulation F) during the early stage of the agglomeration for a 30 nm NiSi film on Si substrate at 600°C. Compared to the simulation D, the grooving process is weakened in simulation F due to the decrease in misorientation between NiSi grains, even if the increase in the NiSi/Si misorientation should accelerate agglomeration in simulation F. This behavior was confirmed by using a bicrystal structure (Figure S6) and the phase-field simulation (Figure S7): the grooving phenomena was faster for high angle grain boundaries even if the misorientation with the substrate is lower. **Figure 6c** shows the early stage of the exposed Si for simulation D and F: when the fraction of exposed Si is less than 3.0%, grooving is the primary microstructure evolution process in this case. The kinetics of the grooving process depends strongly on the misorientation between NiSi grains, but is less sensitive to the volume

fraction of the different misorientations. A small misorientation between the NiSi grains will be an advantage to delaying the grooving of the NiSi grains, and thus the agglomeration.

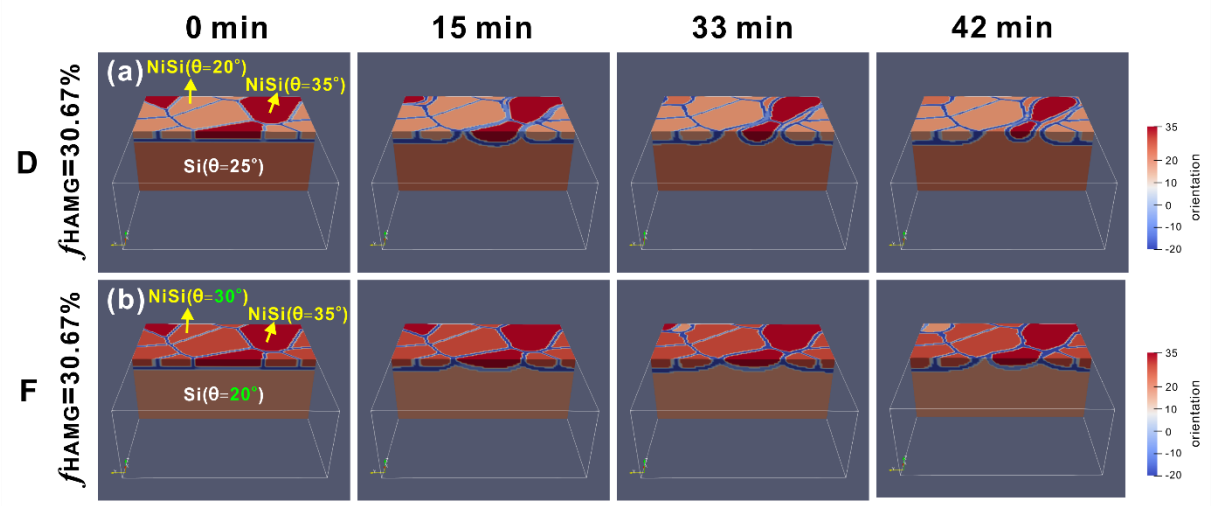

Fig. 8. Longitudinal cross-section of the simulated microstructure evolution for different misorientation distributions with same volume fraction on the agglomeration for 30 nm NiSi film on Si substrate at 600°C: (a) f_{HAMG}=30.67%, with $\theta_{NiSi^2/Si}$ = 5°, $\theta_{NiSi^3/Si}$ = 10°, $\theta_{NiSi^2/NiSi^3}$ = 15°, (b) f_{HAMG}=30.67%, with $\theta_{NiSi^3/Si}$ = 15°, $\theta_{NiSi^4/Si}$ = 10°, $\theta_{NiSi^3/NiSi^4}$ = 5°. Different colors represent the different NiSi orientations, while the Si substrate is transparent.

5.5 Application in real NiSi polycrystalline films

As discussed above, the misorientation distribution and the volume fraction of NiSi grains can strongly affect the agglomeration process in 30 nm NiSi films on a monocrystal Si substrate. In order to better account for the complexity of the NiSi polycrystalline film and compare it with the *in-situ* SEM results, a larger number of NiSi grains with an orientation distribution close to the experimental one was used in the following simulation. The initial microstructure with 107 grains was constructed based on the experimental orientation distribution in **Fig. 4a** and the average grain size in **Fig. 2a** (the details are given in Figure S8)**.** The change of misorientation on the interfacial energies and mobility was calculated based on Eq.(7) and Eq.(8). The simulated domain is 300×300×40 grids, grid size Δx is 5 nm, and the interface thickness is $4\Delta x$. The NiSi film thickness is 30 nm, and the initial average radius of NiSi grains was set to 81.8 nm, which is consistent with the *in-situ* SEM results (**Fig. 2a**). As for the other simulations, periodic boundary conditions were used in the four horizontal directions (west, east, south, north), and isolation conditions at the top and bottom.

Figure 9 shows the microstructure evolution during agglomeration obtained by phase-field simulations and *in-situ* SEM for a 30 nm NiSi film on a monocrystal Si substrate at 600°C. As detailed above, the initial simulated structure was constructed based on the experimental

orientation distribution and the initial experimental grain size. As shown in **Fig. 9a**, the grooving always occurs first in the NiSi boundary with large misorientations between them (large difference in colors). A significant difference of misorientation between the NiSi grains, resulting in a significant difference in energy and mobility of NiSi/NiSi grain boundary, will accelerate the grooving, as discussed in *Section 5.4.* As time evolves, NiSi agglomeration occurs, and the number of exposed Si increases. The shape of the exposed Si first follows the initial NiSi grain boundary and then forms isolated 'holes' (Note: these 'holes' are not true ones since the exposed Si is at the same level as the NiSi [18]). This is in good agreement with the *in-situ* SEM results (**Fig. 9c**).

Meanwhile, some NiSi grains with a small misorientation with the neighboring grains evolve very slowly and give the slow evolution region as the *region A* in **Fig. 9 (a2) or (b2)**. This is also in good agreement with the *in-situ* SEM results as *region A* in **Fig. 9 (c2)**. Subsequently, two types of isolated NiSi grains are formed. An example of isolated B-type NiSi grains is marked in **Fig. 9 (a3) or (b3):** these grains have LAM with the substrate but HAM with the neighboring NiSi grains, and they will remain in the whole agglomeration process due to the low misorientation with the Si substrate. That is in good agreement with the *in-situ* SEM results shown in **Fig. 9 (c3-c5)**. Isolated C-type grains are marked in **Fig. 9 (a3) or (b3)**: they are formed because of large misorientation with neighboring NiSi grains, similar to isolated B-type grains, but they will disappear by diffusion due to large misorientation with the Si substrate. Finally, most of the surface-exposed Si regions connect into a single region, and only a few isolated Si holes remain. To summarize, the phase-field simulation (**Fig. 9b**) can nicely reproduce the grooving and agglomeration behaviors observed in the *in-situ* SEM results.

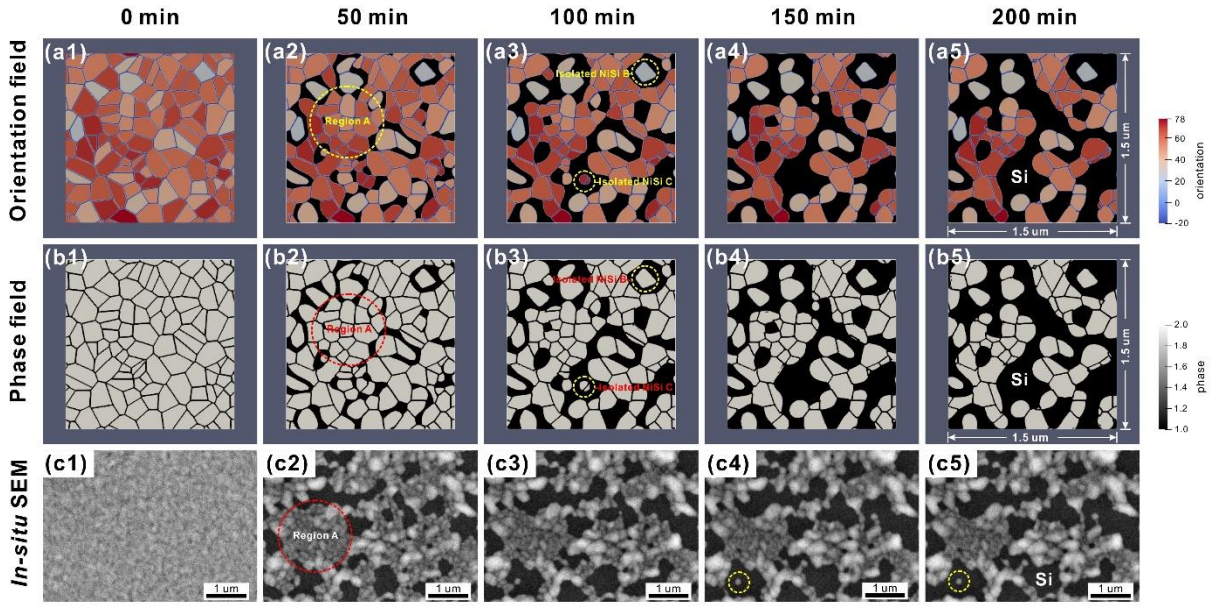

Fig. 9. Microstructure evolution of agglomeration for a 30 nm NiSi film on a monocrystal Si substrate annealing at 600°C: (a) simulation results with orientation field, where different colors represent different orientations of NiSi, and black the Si substrate, (b) simulation results with phase-field, where the gray represents the NiSi phase, and black the exposed Si substrate, (c) *in-situ* SEM results. The initial microstructure for the simulation was constructed by coupling the experimental misorientation distribution from the work of Luo et al. [18] and the initial average grain size from *in-situ* SEM results.

6. Discussion

The phase-field simulations considering the effect of misorientation reproduce well the *in-situ* SEM results. In order to better understand the effect of misorientation on the materials parameter in the simulations and reveal the agglomeration mechanism, more details will be discussed in the following.

In order to explore the agglomeration mechanism, the orientations of NiSi grains and Si substrate were considered in the simulations. In order to simplify the simulations, the NiSi(φ=270°, θ=20°, ψ=90°), which is one of the possible Euler angles for NiSi(103) axiotaxy, was set as the baseline, while the other orientations of the NiSi grains and the Si substrate were set compared to this baseline. Therefore, the misorientation between the NiSi grains and the Si substrate and between the NiSi grains can be easily calculated. The interfacial energies and mobility in each interface depend on the misorientation through Eq.(7) (the Read-Shockley law[42]) and Eq.(8) (the sigmoidal law [43]). For misorientation close to or larger than the high-angle grain boundary θ_{HAB}, the interfacial energy and mobility will tent to the high-angle misorientation value σ_{HAB} and μ_{HAB}. On the contrary, these parameters will tend to zero when the misorientation is low, as shown in Figure S3. For a NiSi grain, the different interfaces will have different interfacial energies and mobilities, which depend on the misorientation of the grains or the phases on both sides of the interface. In simulation B, the NiSi film was constructed by two types of NiSi grains: the LAM NiSi(θ=20°) and the HAM NiSi(θ=35°). The misorientation between NiSi grains of different types is 15° and 0° for NiSi grains of the same type. The orientation of the Si substrate was set as (θ=25°), the misorientation between NiSi(θ=20°) and the Si substrate is 5°, and 10° between NiSi(θ=35°) and the Si substrate. The transition angle misorientation θ_{HAB} was set to 15° for NiSi/NiSi grain boundary and NiSi/Si interface in the simulations B to F. According to Eq.(7) and Eq.(8), the effect of misorientation on the interface energy/grain boundary energy and mobility can be calculated. For the grain boundary with different types of NiSi grains (misorientation is 15°), grain boundary energy and mobility value are $\sigma_{NiSi/NiSi}$ and $\mu_{NiSi/NiSi}$, but are approximate to 0 for the grain boundary with the same type NiSi

grains (misorientation is 0°). The interface energy and mobility for the NiSi/Si interface with HAM (10°) are 0.94· $\sigma_{NiSi/Si}$ and 0.63· $\mu_{NiSi/Si}$, respectively, but are 0.70· $\sigma_{NiSi/Si}$ and 0.06· $\mu_{NiSi/Si}$ for the NiSi/Si interface with LAM (5°). Therefore, the evolution is very slow between NiSi grains with the same orientation. The grooving starts at the grain boundary of NiSi grains with large misorientation, and the evolution of the NiSi/Si interface with HAM is faster than that of the LAM interface, as shown in **Fig. 5b**. These are the main reasons for the agglomeration.

Subsequently, different simulations (simulations B to E) with the different volume fractions of NiSi orientations were performed using the same NiSi grain structure. In simulation B to F, the same NiSi grain structure and two types of NiSi grain orientations are found: the LAM NiSi(θ=20°) and the HAM NiSi(θ=35°), but the volume fraction of HAM NiSi(θ=35°) decreased from 77.25% to 22.65%. The simulations show that the volume fraction of HAM NiSi strongly affects the kinetics of NiSi agglomeration represented by the kinetics of the exposed Si substrate. The simulations show that, for a fraction of HAM grain between 30.67%~56.70%, the kinetics of the surface-exposed Si is in good agreement with the *in-situ* SEM results. In other words, when the fraction of LAMG is 43.30%~69.33%, the kinetics of the exposed Si from the simulations reproduces the *in-situ* SEM results. The fraction of LAMG could be in this range (43.30%~69.33%) for a 30 nm NiSi film on Si(100) substrate at 600°C studied in this work. This is in good agreement with De Keyser *et al.* [8, 9], who measure a total fraction of grains with axiotaxy and epitaxy texture (considered as low-angle grains with low interfacial energy) of 45% and 41% for 60 nm and 90 nm NiSi film.

Moreover, simulations B to E show that the increase in the volume fraction of LAMG, which have low interfacial energies and mobilities, will delay the agglomeration of the NiSi film. These results may provide another good way to explain the reason for the stability improvement of NiSi thin film when alloying Ni with some transition metals, such as W, Ti, Ta [14], and increasing the phase stability of NiSi [12]. For instance, when alloying Ni with W, increasing the W concentration changes the texture: the axiotaxial components decrease, and a particular epitaxial component becomes prominent [14]. Due to the lower interfacial energy for the epitaxial component than the axiotaxial component, the higher the volume fraction of epitaxial NiSi grains, the less likely agglomeration is. The reason for a significant improvement of the morphological stability of 20 nm NiSi on Si(001) by alloying the Ni film with 40% Si[19], which increased the fraction of epitaxial NiSi grains formed by texture inheritance, can also be explained in a similar way.

Furthermore, the effect of different misorientation distributions of NiSi grains on agglomeration was investigated by simulations D and F. Both simulations D and F have the

same NiSi grain structure and volume fraction (30.67%) for the high angle NiSi(θ=35°) grains, but the orientation of low angle NiSi grains was set to NiSi(θ=30°) and the Si substrate was set to (θ=20°) in simulation F. Thus, the misorientation between the different types of NiSi grains is 5° in simulation F. The misorientation between NiSi(θ=30°) and Si(θ=20°) is 10°, 15° between NiSi(θ=35°) and Si(θ=20°). Comparing with simulation D, it is clear that the kinetics of agglomeration in simulation F is faster than that in simulation D in **Fig. 6b**, due to the higher misorientation distribution between NiSi/Si interface: the interface energy and mobility for the NiSi/Si interface with LAM (10°) are $0.94\cdot\sigma_{NiSi/Si}$ and $0.63\cdot\mu_{NiSi/Si}$, and are $\sigma_{NiSi/Si}$ and $\mu_{NiSi/Si}$ for the NiSi/Si interface with HAM (15°) in simulation F. However, for the early stage of simulation, representing the grooving process, the kinetics of the exposed Si in simulation F is slower than that in simulation D, especially for a fraction of exposed Si lower than 3.0%, as shown in **Fig. 6c**. This is due to the decrease in the misorientation between the different types of NiSi grains (from 10° in simulation D to 5° in simulation F). The energy and mobility of the NiSi grain boundary are reduced to $0.70\cdot\sigma_{NiSi/NiSi}$ and $0.06\cdot\mu_{NiSi/NiSi}$. This slows down the evolution between the NiSi grains with different orientations, mainly for the grooving process during the early simulation stage, as shown in **Fig. 8**. Based on the simulation results from simulation B to F in the early stage, it can be clearly found that the grain boundary grooving mainly depends on the misorientation distribution between the NiSi grains. Therefore, reducing the misorientation between individual NiSi grains will delay the grain boundary grooving.

In summary, some suggestions for suppressing or slowing down the agglomeration can be given from texture based on the phase-field simulations: *i*) increase the volume fraction of low angle grains; *ii*) decrease the misorientation between the NiSi grain and the Si substrate; and *iii*) decrease the misorientation between the NiSi grains. The latter will also strongly act on the grooving process. These changes may be achieved using alloy elements.

7. Conclusions

- The microstructure evolution and kinetics of the agglomeration for a 30 nm NiSi film on Si(100) substrate at 600°C were investigated by *in-situ* SEM. During the agglomeration process, most small NiSi grains gradually shrink, except that some specific NiSi grains grow rapidly. The agglomeration of the NiSi grains causes an increase in the exposed Si. Moreover, the evolution of texture of a 30 nm NiSi polycrystalline thin film during agglomeration was investigated by EBSD with *ex-situ* samples, and the results indicated that some fiber texture components remain after long-time annealing while most of the random orientations disappear, which is in good agreement with the previous reports.

- 3-D phase-field simulations were used to reveal the mechanisms of grooving and agglomeration of the NiSi polycrystalline thin film on the monocrystal Si substrate. The simulation results showed that the grooving starts from the NiSi grain boundary with large misorientation, and the kinetics of grooving mainly depends on the misorientation distribution between the NiSi grains. The difference in misorientations of the NiSi/Si and NiSi/NiSi interfaces leads to differences in the interfacial energies and grain boundary energies, which are the main driving forces for agglomeration of the NiSi polycrystalline thin film.
- The 3-D phase-field simulation combined with experimental information (i.e., the orientation distribution and the mean grain size of NiSi grains) well reproduced the complex agglomeration process in 30 nm NiSi polycrystalline films observed by *in-situ* SEM. According to the quantitative phase-field simulations, in order to suppress or to slow down the agglomeration, either increasing the volume fraction of low angle grains, or decreasing the misorientation between the NiSi grain and the Si substrate is recommended.
- In this paper, the coupling of the *in-situ* SEM observations and MPF simulations was successful to reveal the agglomeration mechanism in the NiSi polycrystalline thin film on the monocrystal Si substrate, and can thus serve as an efficient way to bring insights into dewetting phenomena of the polycrystalline thin film.

Acknowledgment

Jianbao Gao acknowledges the China Scholarship Council (CSC NO. 201906370115). Lijun Zhang acknowledges the Youth Talent Project of Innovation-driven Plan at Central South University (Grant No. 2282019SYLB026). The authors acknowledge financial support from the CNRS-CEA ‘‘METSA’’ French network (FR CNRS 3507) for the in situ SEM experiments at CLYM (www.clym.fr), which is also acknowledged for access to the Quattro ESEM (Thermo Scientific).

References

[1] C. Lavoie, F.M. d’Heurle, C. Detavernier, C. Cabral, Towards implementation of a nickel silicide process for CMOS technologies, Microelectron. Eng. 70(2-4) (2003) 144-157.
[2] D. Mangelinck, J.Y. Dai, J.S. Pan, S.K. Lahiri, Enhancement of thermal stability of NiSi films on (100)Si and (111)Si by Pt addition, Appl. Phys. Lett. 75(12) (1999) 1736-1738.
[3] D. Deduytsche, C. Detavernier, R.L. Van Meirhaeghe, C. Lavoie, High-temperature degradation of NiSi films: Agglomeration versus $NiSi_2$ nucleation, J. Appl. Phys. 98(3) (2005) 033526.
[4] B. De Schutter, K. De Keyser, C. Lavoie, C. Detavernier, Texture in thin film silicides and germanides: A review, Appl. Phys. Rev. 3(3) (2016) 031302.

[5] M.R. Anisur, T. Osipowicz, D. Chi, W. Wang, Effects of prolonged annealing on NiSi at low temperature (500°C), J. Electron. Mater. 34(8) (2005) 1110-1114.
[6] F. Geenen, K. van Stiphout, A. Nanakoudis, S. Bals, A. Vantomme, J. Jordan-Sweet, C. Lavoie, C. Detavernier, Controlling the formation and stability of ultra-thin nickel silicides-An alloying strategy for preventing agglomeration, J. Appl. Phys. 123(7) (2018) 075303.
[7] S. Gaudet, P. Desjardins, C. Lavoie, The thermally-induced reaction of thin Ni films with Si: Effect of the substrate orientation, J. Appl. Phys. 110(11) (2011) 113524.
[8] K. De Keyser, C. Detavernier, R.L. Van Meirhaeghe, Characterization of the texture of silicide films using electron backscattered diffraction, Appl. Phys. Lett. 90(12) (2007) 121920.
[9] K. De Keyser, C. Detavernier, R.L. Van Meirhaeghe, J. Jordan-Sweet, C. Lavoie, The texture of thin NiSi films and its effect on agglomeration, in: A.D. Rollett (Ed.), Applications of Texture Analysis, 2008, pp. 1-9.
[10] C. Detavernier, J. Jordan-Sweet, C. Lavoie, Texture of NiSi films on Si(001), (111), and (110) substrates, J. Appl. Phys. 103(11) (2008) 113526.
[11] P. Jacquet, R. Podor, J. Ravaux, J. Lautru, J. Teisseire, I. Gozhyk, J. Jupille, R. Lazzari, On the solid-state dewetting of polycrystalline thin films: Capillary versus grain growth approach, Acta Mater. 143 (2018) 281-290.
[12] C. Lavoie, C. Detavernier, C. Cabral, F.M. d'Heurle, A.J. Kellock, J. Jordan-Sweet, J.M.E. Harper, Effects of additive elements on the phase formation and morphological stability of nickel monosilicide films, Microelectron. Eng. 83(11-12) (2006) 2042-2054.
[13] C. Detavernier, C. Lavoie, Influence of Pt addition on the texture of NiSi on Si (001), Appl. Phys. Lett. 84(18) (2004) 3549-3551.
[14] D. Deduytsche, C. Detavernier, R. Van Meirhaeghe, J. Jordan-Sweet, C. Lavoie, Formation and morphological stability of NiSi in the presence of W, Ti, and Ta alloying elements, J. Appl. Phys. 101(4) (2007) 044508.
[15] T. Luo, D. Mangelinck, M. Descoins, M. Bertoglio, N. Mouaici, A. Hallén, C. Girardeaux, Combined effect of Pt and W alloying elements on Ni-silicide formation, J. Appl. Phys. 123(12) (2018) 125301.
[16] F.A. Geenen, E. Solano, J. Jordan-Sweet, C. Lavoie, C. Mocuta, C. Detavernier, The influence of alloying on the phase formation sequence of ultra-thin nickel silicide films and on the inheritance of texture, J. Appl. Phys. 123(18) (2018) 185302.
[17] C. Detavernier, A. Özcan, J. Jordan-Sweet, E. Stach, J. Tersoff, F. Ross, C. Lavoie, An off-normal fibre-like texture in thin films on single-crystal substrates, Nature 426(6967) (2003) 641-645.
[18] T. Luo, C. Girardeaux, H. Bracht, D. Mangelinck, Role of the slow diffusion species in the dewetting of compounds: The case of NiSi on a Si isotope multilayer studied by atom probe tomography, Acta Mater. 165 (2019) 192-202.
[19] C. Van Bockstael, K. De Keyser, R.L. Van Meirhaeghe, C. Detavernier, J.L. Jordan-Sweet, C. Lavoie, Influence of a transient hexagonal phase on the microstructure and morphological stability of NiSi films, Appl. Phys. Lett. 94(3) (2009) 033504.
[20] M. Bouville, S. Hu, L.-Q. Chen, D. Chi, D.J. Srolovitz, Phase-field model for grain boundary grooving in multi-component thin films, Modell. Simul. Mater. Sci. Eng. 14(3) (2006) 433-443.
[21] M. Bouville, D. Chi, D.J. Srolovitz, Grain-boundary grooving and agglomeration of alloy thin films with a slow-diffusing species, Phys. Rev. Lett. 98(8) (2007) 085503.
[22] I. Steinbach, L. Zhang, M. Plapp, Phase-field model with finite interface dissipation, Acta Mater. 60(6-7) (2012) 2689-2701.
[23] L. Zhang, I. Steinbach, Phase-field model with finite interface dissipation: Extension to multi-component multi-phase alloys, Acta Mater. 60(6–7) (2012) 2702-2710.

[24] L. Zhang, M. Stratmann, Y. Du, S. Bo, I. Steinbach, Incorporating the CALPHAD sublattice approach of ordering into the phase-field model with finite interface dissipation, Acta Mater. 88 (2015) 156-169.
[25] M. Wei, Y. Tang, L.J. Zhang, W.H. Sun, Y. Du, Phase-Field Simulation of Microstructure Evolution in Industrial A2214 Alloy During Solidification, Metall. Mater. Trans. A 46(7) (2015) 3182-3191.
[26] N. Ta, L.J. Zhang, Y. Du, Design of the Precipitation Process for Ni-Al Alloys with Optimal Mechanical Properties: A Phase-Field Study, Metall. Mater. Trans. A 45(4) (2014) 1787-1802.
[27] J. Gao, M. Wei, L. Zhang, Y. Du, Z. Liu, B. Huang, The effect of different initial structure on simulation of microstructure evolution during normal grain growth via phase-field modeling, Metall. Mater. Trans. A 49(12) (2018) 6442-6456.
[28] OIM Analysis™, version 6, 2015, https://www.edax.com/products/ebsd/oim-analysis.
[29] F. Bachmann, R. Hielscher, H. Schaeben, Texture analysis with MTEX–free and open source software toolbox, Solid. State. Phenom. 160 (2010) 63-68.
[30] I. Steinbach, Phase-field models in materials science, Modell. Simul. Mater. Sci. Eng. 17(7) (2009) 073001.
[31] J. Eiken, B. Böttger, I. Steinbach, Multiphase-field approach for multicomponent alloys with extrapolation scheme for numerical application, Phys. Rev. E 73(6) (2006) 066122.
[32] I. Steinbach, F. Pezzolla, A generalized field method for multiphase transformations using interface fields, Physica D 134(4) (1999) 385-393.
[33] J.O. Andersson, T. Helander, L. Höglund, P. Shi, B. Sundman, Thermo-Calc & DICTRA, computational tools for materials science, Calphad 26(2) (2002) 273-312.
[34] MICRESS: The MICRostructure Evolution Simulation Software, version 6.4, 2018, http://www.micress.de.
[35] Y. Du, J.C. Schuster, Experimental investigations and thermodynamic descriptions of the Ni-Si and C-Ni-Si systems, Metall. Mater. Trans. A 30(9) (1999) 2409-2418.
[36] X. Yuan, L. Zhang, Y. Du, W. Xiong, Y. Tang, A. Wang, S. Liu, A new approach to establish both stable and metastable phase equilibria for fcc ordered/disordered phase transition: application to the Al–Ni and Ni–Si systems, Mater. Chem. Phys. 135(1) (2012) 94-105.
[37] F. d'Heurle, S. Petersson, L. Stolt, B. Strizker, Diffusion in intermetallic compounds with the CaF_2 structure: A marker study of the formation of $NiSi_2$ thin films, J. Appl. Phys. 53(8) (1982) 5678-5681.
[38] Y. Du, J.C. Schuster, An effective approach to describe growth of binary intermediate phases with narrow ranges of homogeneity, Metall. Mater. Trans. A 32(9) (2001) 2396-2400.
[39] H. Bracht, E. Haller, R. Clark-Phelps, Silicon self-diffusion in isotope heterostructures, Phys. Rev. Lett. 81(2) (1998) 393.
[40] L.E. Murr, Interfacial phenomena in metals and alloys, Addison-Wesley Publishing Company, United States, 1975.
[41] C. Messmer, J.C. Bilello, The surface energy of Si, GaAs, and GaP, J. Appl. Phys. 52(7) (1981) 4623-4629.
[42] W.T. Read, W. Shockley, Dislocation models of crystal grain boundaries, Phys. Rev. 78(3) (1950) 275.
[43] F. Humphreys, A unified theory of recovery, recrystallization and grain growth, based on the stability and growth of cellular microstructures—I. The basic model, Acta Mater. 45(10) (1997) 4231-4240.

Manuscript (word or pdf w/ figures)